

Nuclear Charge Radii of ${}^8,9\text{Li}$ Determined by Laser Spectroscopy

G. Ewald,¹ W. Nörtershäuser,^{1,2} A. Dax,^{1,*} S. Götze,¹ R. Kirchner,¹ H.-J. Kluge,¹ Th. Kühl,¹ R. Sanchez,¹
A. Wojtaszek,^{1,†} B. A. Bushaw,³ G. W. F. Drake,⁴ Z.-C. Yan,⁵ and C. Zimmermann²

¹*Gesellschaft für Schwerionenforschung, 64291 Darmstadt, Germany*

²*Department of Physics, University Tübingen, D-72076 Tübingen, Germany*

³*Pacific Northwest National Laboratory, P.O. Box 999, Richland, Washington 99352, USA*

⁴*Department of Physics, University of Windsor, Windsor, Ontario N9B 3P4, Canada*

⁵*Department of Physics, University of New Brunswick, Fredericton, New Brunswick E3B 5A3, Canada*

(Received 20 May 2004; published 9 September 2004)

The $2s \rightarrow 3s$ transition of ${}^{6,7,8,9}\text{Li}$ was studied by high-resolution laser spectroscopy using two-photon Doppler-free excitation and resonance-ionization detection. Hyperfine structure splittings and isotope shifts were determined with precision at the 100 kHz level. Combined with recent theoretical work, the changes in the nuclear-charge radii of ${}^{8,9}\text{Li}$ were determined. These are now the lightest short-lived isotopes for which the charge radii have been measured. It is found that the charge radii monotonically decrease with increasing neutron number from ${}^6\text{Li}$ to ${}^9\text{Li}$.

DOI: 10.1103/PhysRevLett.93.113002

PACS numbers: 32.10.Fn, 21.10.Ft, 27.20.+n

Laser spectroscopy is an important tool for model-independent determination of nuclear properties for short-lived isotopes, giving information on collective and single-particle effects [1,2]. Nuclear spins and moments can be extracted from the hyperfine structure (HFS) in an optical transition and differences in nuclear-charge radii $\delta\langle r_c^2 \rangle$ can be derived from isotope shift (IS) determinations. The latter requires separation of effects caused by changes in mass and in nuclear-charge volume. For lighter elements the mass shift is large, while the so-called volume or field shift is small: For Li the volume shift is only on the order of 10^{-4} of the total IS. It is also necessary to account for electron correlation effects, which cause a state-specific mass shift (SMS) in addition to the normal Bohr mass shift. Until recently, the SMS could not be calculated with sufficient accuracy for atomic systems with more than two electrons. Therefore, determinations of nuclear-charge radii for light atoms ($Z < 10$) have been restricted to stable isotopes, either by electron scattering or by investigating muonic atoms [3], or to hydrogen and helium isotopes by optical spectroscopy.

Recently, it has become possible to perform highly accurate calculations for the three-electron system of neutral lithium [4–6] and to test these results by optical spectroscopy on the stable isotopes ${}^{6,7}\text{Li}$ [7], where comparison can be made with r_c values known from electron scattering. This new theoretical development now allows the evaluation of optical IS data for determination of r_c for the radioactive lithium isotopes, with the prospect of reaching the neutron drip line at $A = 11$ and obtaining a first-time r_c measurement for ${}^{11}\text{Li}$, the most prominent neutron halo nucleus. To do so, we have developed a novel on-line laser and mass spectroscopic technique which combines extreme accuracy with high sensitivity. Here, we present the first application of this method and report

measurement of the IS between the stable isotopes ${}^{6,7}\text{Li}$ and the short-lived isotopes ${}^{8,9}\text{Li}$, making these the lightest radioisotopes for which model-independent r_c have been determined. A decrease in r_c is observed with increasing mass number, and this is compared with the predictions of various nuclear models.

The experimental arrangement is shown in Fig. 1. The short-lived isotopes with half-life $T_{1/2} = 838$ ms (${}^8\text{Li}$) and 178.3 ms (${}^9\text{Li}$) are produced at the on-line mass separator at GSI, Darmstadt, by directing an 11.4 MeV/u ${}^{12}\text{C}$ beam from the UNILAC onto a 100 mg/cm² tungsten target. Fast reaction products enter the hot ion source of the mass separator through a tung-

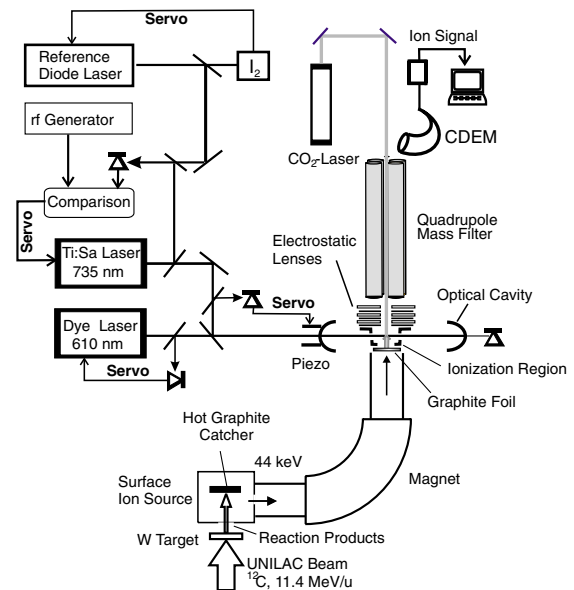
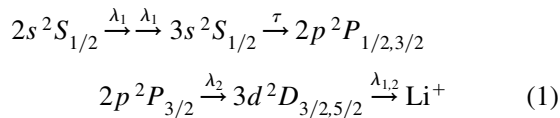


FIG. 1 (color online). Experimental setup.

sten window and are stopped in a sintered graphite catcher. Atoms diffusing out of the catcher are surface ionized and extracted through a small hole. After acceleration to 44 keV the ions are mass separated and delivered to the experiment. Maximum yields were about 200 000/s for ^8Li and 100 000/s for ^9Li .

The Li ions from the mass separator are stopped near the far surface of a thin graphite foil ($80 \mu\text{g}/\text{cm}^2$) that is heated to 1800–1900 °C with a CO_2 laser ($\sim 4 \text{ W}$). The implanted lithium diffuses quickly out of the foil and drifts into the ionization region of a quadrupole mass spectrometer (QMS). Here the Li atoms are laser ionized; the ions are mass analyzed with the QMS and detected with a continuous dynode electron multiplier (CDEM). The overall excitation



is performed with cw single-mode lasers, where $\lambda_1 = 735 \text{ nm}$ is provided by a titanium-sapphire (Ti:Sa) laser, $\lambda_2 = 610 \text{ nm}$ by a dye laser, and $\tau = 29.8 \text{ ns}$ is the spontaneous decay lifetime of the $3S$ state [8]. This scheme was chosen to achieve the required resolution in the $2s \rightarrow 3s$ Doppler-free two-photon transition, as well as high ionization efficiency for sensitive detection. Within this scheme, the $3s \rightarrow 2p$ spontaneous decay decouples the high-resolution spectroscopy from the resonantly enhanced ionization via the $3D$ states. Relatively high laser intensities are needed to approach saturation in both steps of the process. Therefore both lasers are enhanced by a factor of ~ 100 within a resonant optical cavity. To couple both lasers into the cavity, the resonator is locked to the Ti:Sa laser, while the dye laser is locked to the resonator. Hence, the dye laser frequency does not exactly match a $2p \rightarrow 3d$ resonance. However, at typical intensities of $\sim 17 \text{ W}/\text{mm}^2$, the $2p \rightarrow 3d$ transitions were broadened to $\sim 8 \text{ GHz}$, and the two $3D$ fine structure components overlap to form a peak with an $\sim 1.2 \text{ GHz}$ flat-top region. The free spectral range of the resonator is $\sim 500 \text{ MHz}$ and thus a lock point with good ionization efficiency can always be found. The final ionization step can occur by absorption of either a 610 nm or a 735 nm photon.

The Ti:Sa laser is stabilized by frequency-offset locking to a diode-laser reference system that is locked to an iodine line [$X^1\Sigma_g^+ \rightarrow BO_u^+R(114)11-2, a_1$] using frequency modulation saturation spectroscopy [9]. The beat frequency between the two lasers is detected with a 25 GHz bandwidth photodiode and serves as the basis for a servo loop controlling the Ti:Sa laser frequency. Typical linewidths of the beat signal were $\sim 1 \text{ MHz}$.

The following measurement procedure was used: The Ti:Sa laser was set to a desired frequency and the ion beam turned on for 10 s. Laser-ionized atoms were detected during this period and for an additional 5 s (^8Li) or

1 s (^9Li). This additional time is $> 5T_{1/2}$ for the respective isotope and allows decay of radioactive particles implanted into the CDEM. Typical scans recorded data at 1 MHz steps over $\pm 15 \text{ MHz}$ about the expected resonance positions. Reference spectra for both stable isotopes were regularly interspersed among the radioisotope measurements.

Figure 2 shows typical spectra recorded for the Li $2s \rightarrow 3s$ transition. Figure 2(a) shows the overall structure for ^7Li with two hyperfine transitions ($\Delta F = 0, F = 1, 2$). The fitting function is a sum of a Gaussian pedestal, corresponding to the absorption of two photons from the same direction, and a Voigt profile for the narrow component. The Doppler-free peak has a Lorentzian width of 3 to 5 MHz depending on laser power. Without saturation broadening a width of 2.7 MHz would be expected from the lifetime of the $3S$ level. The Gaussian component showed no power dependence and was $\sim 2 \text{ MHz}$, slightly larger than the typical laser linewidth. The pedestal Gaussian width of $\sim 3 \text{ GHz}$ corresponds to the normal Doppler width constrained by the geometry of the interaction region. Figures 2(b) and 2(c) show scans for ^8Li and ^9Li , respectively. The solid lines are fits using the same line function as in Fig. 2(a) but with fixed width for the underlying Gaussian profile. To obtain IS values with an accuracy of a few 100 kHz, systematic effects on the line positions must be identified. Therefore, off-line test measurements with the stable isotopes $^6,7\text{Li}$ were per-

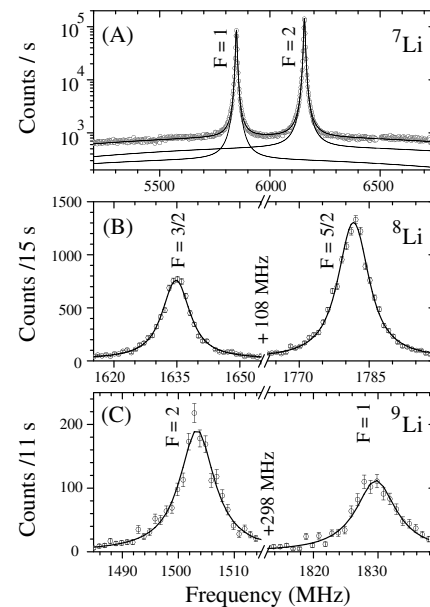


FIG. 2. Resonance-ionization spectra of $^{7,8,9}\text{Li}$. (a) Overall spectrum and line shape for ^7Li . “Skip-step scans” were used for ^8Li (b) and ^9Li (c) splitting determinations, with the size of the skipped frequency range indicated at the breaks. The frequency axis is the beat frequency between the reference laser and the Ti:Sa laser with $\nu_{\text{Ti:Sa}} < \nu_{\text{Ref}}$ (a),(b) and $\nu_{\text{Ti:Sa}} > \nu_{\text{Ref}}$ (c).

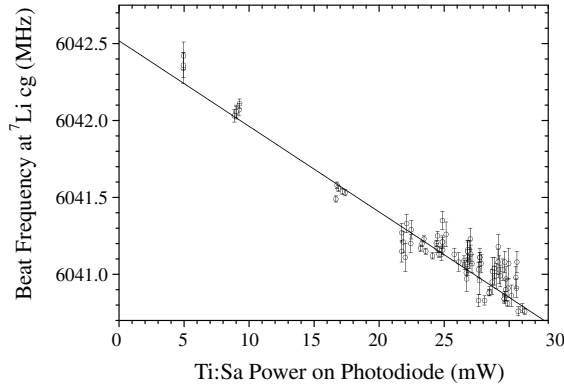


FIG. 3. ${}^7\text{Li}$ HFS center of gravity as a function of the Ti:Sa laser power at the exit of the enhancement cavity. The line is a linear fit to the data points weighted by their uncertainty.

formed altering various operating conditions. These included intensities of the two excitation lasers, relocking of the diode-laser, and changing the iodine reservoir temperature. Only the intensity of the Ti:Sa laser was found to have a statistically significant influence on the center frequencies. To correct for this power shift, a photodiode was placed behind the end mirror of the enhancement cavity, and transmitted light intensity was recorded during each scan. Spectra were taken with varying laser powers and observed absolute resonance positions were blueshifted (manifested as a decreased beat frequency for ${}^7\text{Li}$) with linear dependence on the cavity-enhanced Ti:Sa laser intensity (Fig. 3). In contrast, the observed splittings (HFS and IS) were unchanged. The slopes, corresponding to ac Stark shift coefficients, were found to be equal (within fitting uncertainty of $\sim 3\%$) for ${}^6\text{Li}$, ${}^7\text{Li}$, and ${}^8\text{Li}$. A similar dependence is expected for ${}^9\text{Li}$.

The observed HFS splitting $\Delta\nu_{2S\rightarrow 3S}$ in the transition can be combined with previously measured ground state (gs) splittings $\Delta\nu_{2S}$ from the literature [10–12] to calculate the A factors of the $3S$ states:

$$A_{3S}(i\text{Li}) = (\Delta\nu_{2S\rightarrow 3S}^i - \Delta\nu_{2S}^i)/(I_i + 1/2), \quad (2)$$

where I_i is the nuclear spin of isotope i . Results are listed in Table I. The ${}^6,7\text{Li}$ values agree well with previous measurements [7], while the ${}^8,9\text{Li}$ values have been determined for the first time. The accuracy for ${}^9\text{Li}$ is limited by uncertainty in the ground state hyperfine splitting [12]. Therefore the ${}^9\text{Li}$ gs splitting was calculated from our results and the gs splitting of ${}^8\text{Li}$ assuming no hyperfine anomaly. The result of 848.28(17) MHz was then used to calculate the A factor for the $3S$ state listed in Table I. The given uncertainty allows for a possible hyperfine anomaly of 10^{-4} in addition to the measurement uncertainty.

To determine isotope shifts, the center of gravity (cg) of the HFS transitions was calculated using $\nu_{\text{cg}} = (C_F\nu_{F'} - C_{F'}\nu_F)/(C_{F'} - C_F)$, where C_F and $C_{F'}$ are

TABLE I. Hyperfine structure constants A for the $3S$ states of ${}^{6,7,8,9}\text{Li}$. All values are in MHz.

${}^6\text{Li}$	${}^7\text{Li}$	${}^8\text{Li}$	${}^9\text{Li}$	Reference
35.283(10)	93.117(25)	35.496(28)	98.39(12)	This work.
35.263(15)	93.106(11)			[7]
35.250	93.09	35.453	98.31	[13] ^a

^aTheoretical work in combination with known magnetic moments.

Casimir coefficients for states with total angular momentum F and F' . For each ${}^{6,8,9}\text{Li}$ measurement, the laser power was determined and used to calculate the ${}^7\text{Li}$ reference position from the linear ac Stark shift function shown in Fig. 3. The resulting IS $\Delta\nu_{\text{exp}}^{A,7}$ showed no systematic trends when plotted against either time or laser power. Thus, the final IS values listed in Table II are the statistically weighted average of all measurements with uncertainties given as the standard error of the mean for sets of 62 (${}^6\text{Li}$) and 104 (${}^{8,9}\text{Li}$) measurements. An additional uncertainty of 110 kHz has been added linearly to allow for systematic error in the ac Stark shift correction. The IS for ${}^6\text{Li}$ agrees within 1.3σ with a previous measurement on this transition [7].

The change in nuclear-charge radii is related to the measured IS by [4]

$$\delta\langle r_c^2 \rangle^{A,7} = \frac{\Delta\nu_{\text{exp}}^{A,7} - \Delta\nu_{\text{MS,theo}}^{A,7}}{C}, \quad (3)$$

where $\Delta\nu_{\text{MS,theo}}^{A,7}$ are the calculated mass shifts and $C = -1.5661$ MHz/fm² is the field shift constant for the Li $2s \rightarrow 3s$ transition taken from [5]. Results for $\delta\langle r_c^2 \rangle$ are included in Table II. For the stable isotopes, $\delta\langle r_c^2 \rangle^{6,7} = 0.61(11)$ fm² agrees with a previous determination using the same transition [0.47(5) fm² [7]] within the combined uncertainties and is also in agreement with the electron scattering result of 0.79(25) fm² [14].

The rms charge radii r_c were calculated according to $r_c(A\text{Li}) = [r_c^2({}^7\text{Li}) + \delta\langle r_c^2 \rangle^{A,7}]^{1/2}$, where $r_c({}^7\text{Li})$ obtained from electron scattering [14] is used as the reference. Results are plotted in Fig. 4 and compared with various theoretical predictions. A clear trend to smaller r_c with increasing neutron number can be observed. This may be

TABLE II. Isotope shift $\Delta\nu_{\text{exp}}^{A,7}$ of the $2^2S_{1/2} \rightarrow 3^2S_{1/2}$ transition and extracted $\delta\langle r_c^2 \rangle^{A,7}$ and rms r_c values.

	IS, MHz	$\delta\langle r_c^2 \rangle^{A,7}$, fm ²	r_c , fm	Reference
${}^6\text{Li}$	-11 453.95(13)	0.61(11)	2.51(6)	This work.
	-11 453.734(30)	0.47(5)	2.49(4)	[7]
		0.79(25)	2.55(4)	[14]
${}^7\text{Li}$			2.39(3)	[14]
${}^8\text{Li}$	8 635.79(15)	-0.45(15)	2.29(8)	This work.
${}^9\text{Li}$	15 333.14(18)	-0.78(17)	2.22(9)	This work.

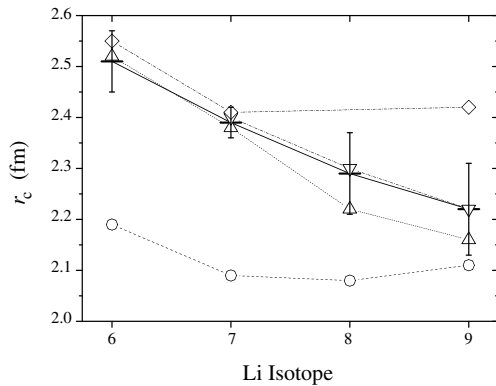


FIG. 4. The rms charge radii for ${}^{6,7,8,9}\text{Li}$: (+) this measurement with ${}^7\text{Li}$ r_c from electron scattering as reference; (O) LBSM [18]; (Δ) QMC [16,17]; (∇) SVMC [15]; (\diamond) DCM [19].

explained by the clustered structure of the Li nuclei ${}^6\text{Li}$ ($\alpha + d$) and ${}^{7-11}\text{Li}$ ($\alpha + t + n + \dots + n$) [15], which diminishes when more neutrons are added, resulting in a more compact nucleus. Stochastic variational multi-cluster (SVMC) calculations [15] and quantum Monte Carlo calculations (QMC) [16,17] clearly reproduce this trend, and also the absolute values are in good agreement with our results. This shows that the fundamental treatment of light nuclei using nucleon-nucleon interactions has reached a high level of accuracy. In contrast, large-basis shell-model (LBSM) calculations underestimate the absolute size and predict a minimum r_c at $A = 8$ [18]. The dynamic-correlation model (DCM) reproduces r_c for the two stable nuclei quite well, but the radius for ${}^9\text{Li}$ is predicted to be larger than that of ${}^7\text{Li}$ [19]. Neither of these latter two models is in accordance with our results. Experimentally, nuclear-model dependent values for r_c also have been extracted from measured interaction cross sections [20] and exhibit the trend to smaller r_c with increasing neutron number, in qualitative agreement with the current study.

To conclude, we have demonstrated that high-resolution cavity-enhanced two-photon spectroscopy in combination with resonance-ionization and mass spectrometry yields the required sensitivity for on-line experiments. The technique was applied to ${}^{8,9}\text{Li}$, and, in combination with advanced atomic calculations, the small nuclear volume effect could be extracted. A steady decrease of the charge radii with increasing mass number was observed, allowing discrimination between different nuclear models. The new method presented here will also allow a determination of the charge radius of ${}^{11}\text{Li}$ in the near future.

We thank F. Schmitt and H. Wang for their contributions in the early stages of the experiment, and K. Burkhard and W. Hüller for beamtime support. This

work is supported by BMBF Contract No. 06TU203. B. A. B. acknowledges support from the U.S. DOE under Contract No. DE-AC06-76RLO 1830, and G.W.F.D. and Z.-C.Y. acknowledge support from NSERC and SHARCnet.

*Present address: CERN, CH-1211 Geneva 23, Switzerland.

†Present address: Faculty of Physics, Warsaw University PL-00-681, Poland.

- [1] E. W. Otten, in *Treatise on Heavy-Ion Science*, edited by D. A. Bromley (Plenum Press, New York, 1989), Vol. 8, p. 517.
- [2] H.-J. Kluge and W. Nörtershäuser, *Spectrochim. Acta, Part B* **58**, 1031 (2003).
- [3] G. Fricke, C. Bernhardt, K. Heilig, L. A. Schaller, L. Schellenberg, E. B. Shera, and C. W. de Jager, *At. Data Nucl. Data Tables* **60**, 177 (1995).
- [4] Z.-C. Yan and G. W. F. Drake, *Phys. Rev. A* **61**, 022504 (2000).
- [5] Z.-C. Yan and G. W. F. Drake, *Phys. Rev. A* **66**, 042504 (2002).
- [6] Z.-C. Yan and G. W. F. Drake, *Phys. Rev. Lett.* **91**, 113004 (2003).
- [7] B. A. Bushaw, W. Nörtershäuser, G. Ewald, A. Dax, and G. W. F. Drake, *Phys. Rev. Lett.* **91**, 043004 (2003).
- [8] M. Godefroid, C. F. Fischer, and P. Jönsson, *J. Phys. B* **34**, 1079 (2001).
- [9] W. Nörtershäuser *et al.*, *Nucl. Instrum. Methods Phys. Res., Sect. B* **204**, 644 (2003).
- [10] E. Arimondo, M. Inguscio, and P. Violino, *Rev. Mod. Phys.* **49**, 31 (1977).
- [11] R. Neugart, *Z. Phys.* **261**, 237 (1973).
- [12] E. Arnold, J. Bonn, R. Gegenwart, W. Neu, R. Neugart, E. W. Otten, G. Ulm, K. Wendt, and the ISOLDE Collaboration, *Phys. Lett. B* **197**, 311 (1987).
- [13] Z.-C. Yan, D. K. McKenzie, and G. W. F. Drake, *Phys. Rev. A* **54**, 1322 (1996).
- [14] C. W. de Jager, H. deVries, and C. deVries, *At. Data Nucl. Data Tables* **14**, 479 (1974).
- [15] Y. Suzuki, R. G. Lovas, and K. Varga, *Prog. Theor. Phys. Suppl.* **146**, 413 (2002).
- [16] S. C. Pieper, K. Varga, and R. B. Wiringa, *Phys. Rev. C* **66**, 044310 (2002).
- [17] S. C. Pieper and R. B. Wiringa, *Annu. Rev. Nucl. Part. Sci.* **51**, 53 (2001).
- [18] P. Navrátil and B. R. Barrett, *Phys. Rev. C* **57**, 3119 (1998).
- [19] M. Tomaselli, T. Kühn, W. Nörtershäuser, G. Ewald, R. Sanchez, S. Fritzsche, and S. G. Karshenboim, *Can. J. Phys.* **80**, 1347 (2002).
- [20] I. Tanihata, T. Kobayashi, O. Yamakawa, S. Shimoura, K. Ekuni, K. Sugimoto, N. Takahashi, T. Shimoda, and H. Sato, *Phys. Lett. B* **206**, 592 (1988).